REVIEW

Electrochemistry at synchrotrons

Zoltán Nagy

Abstract Synchrotron techniques (X-ray and far infrared) have been used in electrochemical research for about the last 25 years. They are powerful new tools to investigate in situ the structure of the electrochemical interphase extending a few thousand angstrom in both phases around the solid/liquid interface. A brief description of the experimental techniques is given, with numerous examples of their applications to investigate a wide variety of phenomena, including measurements of the roughness of electrode surfaces such as relaxation/reconstruction of metal surfaces, the structure of the electrochemical double layer, adsorption/absorption at electrode surfaces, oxide film formation on metals and passivation, underpotential deposition of metals, electrode structures/compositions in batteries and fuel cells, and porous electrode surfaces such as anodic formation of porous silicon. Some historical notes and personal reminiscences are also included.

Keywords Synchrotron X-ray techniques · Far infrared · Electrochemical interphase · Structure of the electrochemical double layer · Adsorption/absorption · Electrode phenomena · Underpotential deposition

Z. Nagy (✉)
Department of Chemistry, University of North Carolina at Chapel Hill,
Chapel Hill, NC 27599, USA
e-mail: nagyz@email.unc.edu

Z. Nagy
Chemical Engineering Department, Case Western Reserve University,
Cleveland, OH 44106, USA

Introduction

Synchrotron techniques became part of electrochemistry's arsenal of investigative tools only relatively recently with the beginning of a new phase of electrochemistry dominated by "surface-science/catalysis." This phase of electrochemistry follows the "thermodynamics/solution-chemistry" dominated phase lasting until about the 1950s and the "kinetics/mechanism" dominated phase lasting until about the 1980s. The first papers reporting the application of synchrotron X-ray techniques in electrochemistry were presented at a symposium on passivity in 1983 [1].

The central phenomenon of electrochemistry, the transfer of charge between an electronically conducting phase and an ionically conducting phase, always occurs at a phase boundary—an interface—between the two phases. The region of interest, however, is usually wider than a simple two-dimensional interface. The atomic-level structure of both phases at the interface can be drastically different from those of the bulk structures. These "special regions" can penetrate from a few angstrom to a few thousand angstrom in both phases. To emphasize the three-dimensional nature

of this region of interest, it is often called the *interphase*. The most common combination is a solid metal/aqueous solution interphase, although numerous other possibilities also exist. The important effect of the state of the metal surface on the rate and mechanism of charge-transfer reactions was recognized at the very earliest times of electrochemical research. Special "active surface sites" were proposed to explain many experimental observations, and great care was taken to use "reproducible surface preparation" techniques. However, real understanding of these "surface effects" was very much hampered by the virtual absence of experimental techniques for the determination of the *atomic-* and *molecular-level* structure of the interphase, both in the morphological and in the chemical sense. The situation has changed considerably in recent decades with the development of UHV surface science, modern spectroscopic techniques, and the discovery of scanning tunneling microscopy and related techniques. Numerous approaches have been tried for the investigation of electrochemical interphases both ex situ and in situ. In the past, the ex situ techniques were used more often than the in situ techniques, but this tendency has now been reversed. While much useful information can be obtained using the ex situ techniques, there always remains a nagging doubt about the effect the loss of potential control and the changing environment from metal/solution to metal/vacuum may have had on the surface conditions. In contrast, the in situ techniques, while experimentally more difficult, overcome these disadvantages. Namely, they permit the continuous electrochemical control of the interphase during the structural/chemical examination (permitting also dynamic measurements under changing electrochemical conditions), and they retain the aqueous condition during the measurement.

The experimental difficulties of in situ techniques stem from the special nature of the electrochemical interphase, namely, that it is a *buried interface* and the probe used for the investigation must be able to penetrate either the electronically conducting phase or the ionically conducting phase. Consequently, the probe must fulfill certain criteria: (1) The probe's interaction with the atoms in the interphase under investigation, at the probe's incident flux, must be sufficiently strong to be surface/interface sensitive, and (2) the interaction of the probe with at least one of the phases must be sufficiently weak for penetration to and from the interface without significant intensity loss. Among the atomic-level structural probes—neutrons, electrons, and X-rays—only synchrotron X-rays meet both criteria for the in situ investigation of electrochemical interphases. The first criterion is fulfilled because of the much larger flux of the synchrotron X-rays compared with that of the older X-ray sources (Fig. 1), and the second criterion is met by the large penetration depth of hard X-rays in water (Fig. 2).
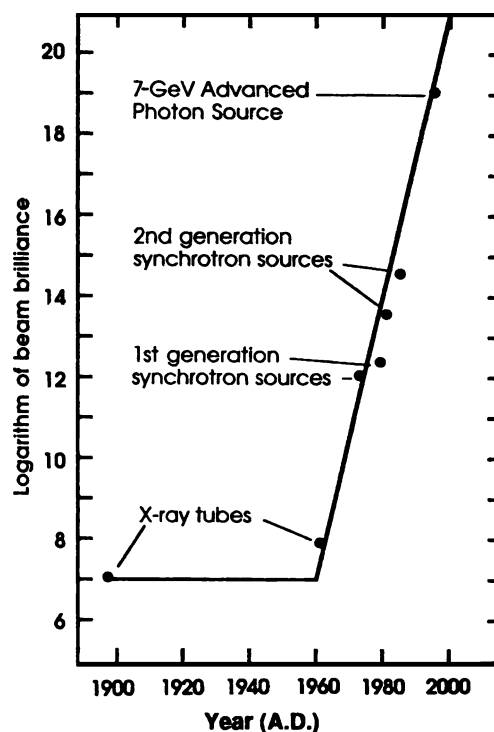

Fig. 1 Historical increase of X-ray source brilliance

Synchrotrons are relatively new and very powerful sources of X-ray radiation. They are based on the phenomenon that when a charged particle undergoes acceleration, electromagnetic waves (in a continuous and wide range of frequencies) are generated. A particle in a circular orbit experiences acceleration toward the center of the orbit and consequently emits radiation in an axis perpendicular to the motion. A synchrotron is a large circular accelerator (storage ring) where electrons (or positrons), inserted from a linear accelerator, are kept orbiting at relativistic speeds. The path of the particles is controlled by magnets, and they are maintained in orbit by the energy supplied through radio-frequency generators.
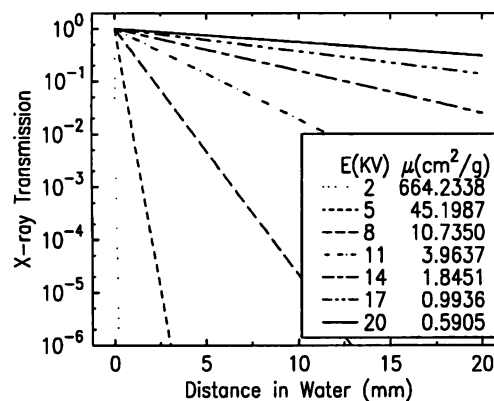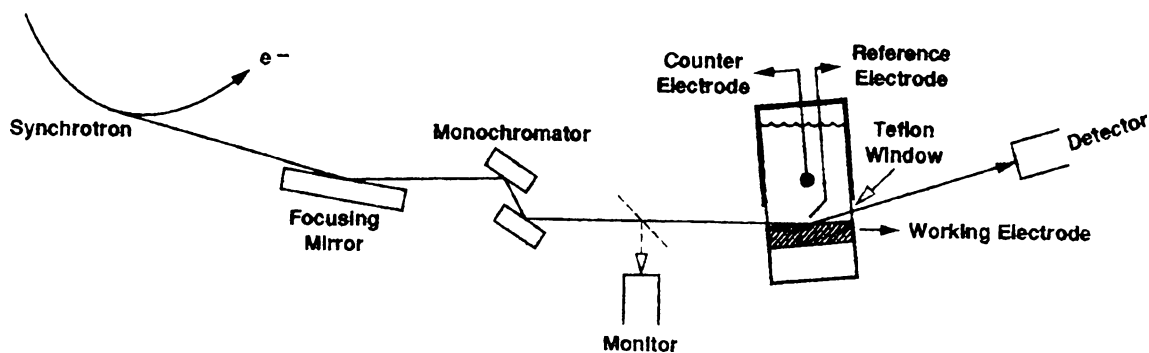

Fig. 2 Transmission coefficient of X-rays versus the distance in water the X-rays travel

Fig. 3 A schematic diagram of the experimental setup for the electrochemical cell and the beamline at the synchrotron

Interspersed around the ring are the so-called insertion devices that extract and direct the radiation into "beamlines," which contain the devices forming the X-ray beam and an experimental station for users. A schematic of the arrangement is shown in Fig. 3.

There are numerous reviews describing the physics and operation of synchrotrons and the theories, experimental details, and data-evaluation methods of the X-ray techniques used at synchrotrons. Some of these reviews can be found in the references listed [2–9]. In this paper, only a brief description is given of the experimental techniques with a number of examples illustrating their wide range of applicability for investigating the electrochemical interphase.

X-ray absorption spectroscopy including EXAFS and XANES

In contrast to other X-ray techniques used in electrochemistry, this technique is mostly used to obtain bulk structure information, though it can also be used in a surface mode. In these experiments, one measures the change in the absorbance of the sample as the X-ray energy is scanned. The absorbance typically declines smoothly as the energy increases until the energy becomes sufficient to excite a core level electron of the absorbing atom to an unoccupied orbital, then a sudden increase of the absorption occurs, which is called an "absorption edge." The absorption at and above the edge provides a wealth of information about the absorbing atom and its surroundings. The position of the edge itself provides information about the oxidation state of the absorber, while the following oscillatory decline gives structural information. The region closest to the absorption edge is called the X-ray absorption near edge structure (XANES). This region extends to approximately 50 eV above the absorption edge. This fine structure is due to core-level transition of the ejected photoelectron, which, due to its low kinetic energy, probes the unoccupied states in the vicinity of the Fermi level, thus permitting the determination of d band occupancy, an important parameter in electrocatalysis. Due to the long-

range interactions of the photoelectrons, the shape of the XANES spectra can provide important insights into the changes in long-range order, such as octahedral to tetrahedral transitions. Furthermore, for thin film samples, where the beam passes through the entire sample, the edge height is directly proportional to the film thickness. The region between about 50 and 1,000 eV above the absorption edge is called the extended X-ray absorption fine structure (EXAFS). This region contains information about the immediate surroundings around the absorbing atom, such as the identity, distance, and number of neighboring atoms. This region arises because as the X-ray is absorbed, an ejected photoelectron wave is produced, which is backscattered by the neighboring atoms. The interference between the photoelectron wave and the backscattered wave produces the
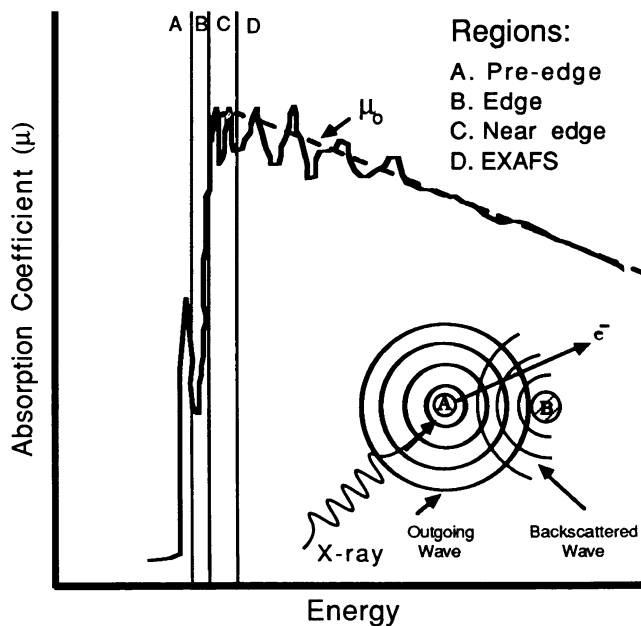
Fig. 4 The various regions in an XAS spectrum; *dashed line* indicates absorption in absence of near neighboring atoms; *inset* origin of EXAFS (Reproduced with permission from Ref. [2], Copyright 1991 by Wiley-VCH)

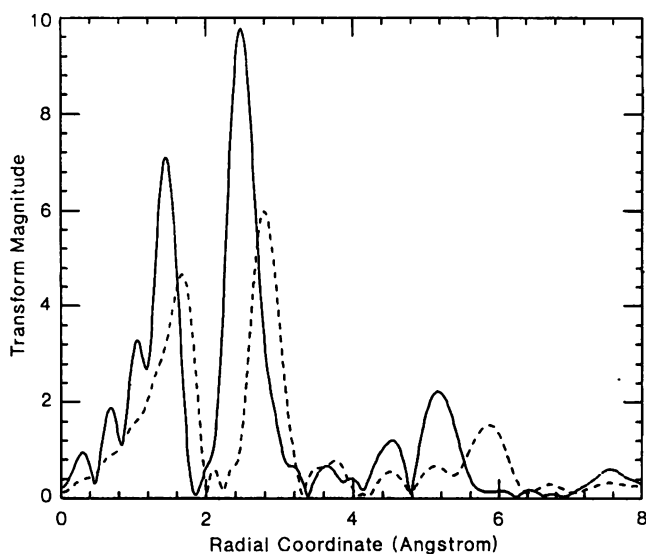oscillations in the absorbance. A schematic representation is shown in Fig. 4.

Investigation of the Ni(OH)$_2$ battery electrode

The structural changes occurring during charging/discharging of a Ni(OH)$_2$ electrode were investigated in strongly alkaline solutions [10]. The EXAFS data (Fig. 5) indicated that the Ni(OH)$_2$ layers in the brucite structure undergo a contraction during oxidation to NiOOH; the octahedral coordination around the Ni undergoes a tetragonal distortion resulting in four short Ni–O bonds (1.88Å) and two longer (2.07Å) bonds with the coordination number changing from six to closer to four. The XANES results (Fig. 6) confirmed these conclusions; the white line was lower in the oxidized material because of the distortion of the symmetry. This is a good example to illustrate the capability of the techniques to determine the short-range order around a central atom (coordination numbers and bond distances), even though the long-range structures are highly disordered.
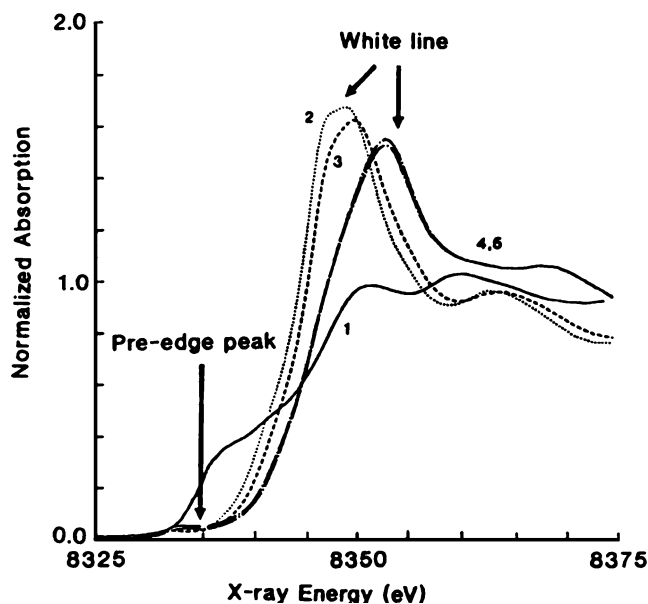
Investigation of the structure and behavior of passive films on metals

The XANES investigation of passive films is reviewed in Ref. [11] with an example as follows.

The protective quality of passive films is determined both by their ability to hinder the flux of ions from the metal substrate to the electrolyte and the stability of the passive film itself (its dissolution rate). The influence of
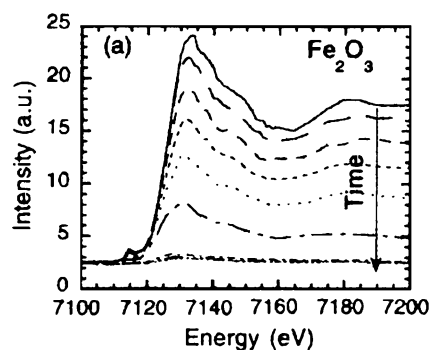

Fig. 6 The XANES results for the K edges of nickel foil (*1*), ex situ data for the uncharged electrode (*2*), and in situ results after the first discharge (*3*), after the first charge (*4*), and second charge (*5*) of the Ni (OH)$_2$ electrode (Reproduced with permission from Ref. [10], Copyright 1995 by World Scientific)

different electrolytes was investigated on the dissolution behavior of Fe, Cr, and Fe/Cr oxide films as a function of the pH of the solution and the presence of halides and EDTA. These aggressive species were found to strongly reduce the stability of Fe$_2$O$_3$ and mixed Fe/Cr oxide films against reductive dissolution. An example of relatively high dissolution rates is the galvanostatic reduction of the passive film on iron in borate buffer (Fig. 7).

When the spectra of Fig. 7 are normalized to the peak height (Fig. 8), there is a gradual shift of the edge in the negative direction, indicating the conversion of the Fe$_2$O$_3$ into an oxide film with a valency near to Fe$_3$O$_4$. In addition to the conversion reaction, dissolution as Fe^{2-} ions occurs, but, in contrast with other reports, a reduction step into metallic iron was not observed.

Fig. 5 A comparison of the evaluated EXAFS results for charged (*solid*) and discharged (*dashed*) Ni(OH)$_2$ electrode. The peak at ~1.5Å is the Ni–O contribution, while the ~2.7 and ~5Å peaks are the first and the third Ni−Ni coordination shells (Reproduced with permission from Ref. [10], Copyright 1995 by World Scientific)
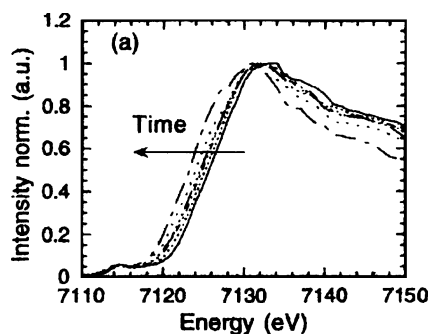

Fig. 7 Consecutive XANES spectra of an originally 21-nm Fe$_2$O$_3$ film during galvanostatic reduction with 5 mA/cm^2 (Reproduced with permission from Ref. [11], Copyright 2002 by Elsevier)

Fig. 8 Details of the XANES spectra of Fig. 7, which have been normalized to the peak height (Reproduced with permission from Ref. [11], Copyright 2002 by Elsevier)

Investigation of fuel cell electrocatalysts

A detailed review of the use of XANES and EXAFS for the investigation of a wide variety of fuel cell catalysts has been published recently [12]. An example of the type of information obtainable with these techniques is an investigation of Sn addition to carbon-supported Pt electrocatalysts. "Carbon-supported platinum (Pt/C) with an adsorbed layer of underpotential (upd) deposited Sn is a much better catalyst for the methanol oxidation reaction (MOR) than a carbon-supported platinum–tin (PtSn/C) alloy. In situ X-ray absorption (XAS) was used to determine the differences in the effects that the two methods of Sn addition have on the electronic properties and the structural properties of the catalyst. X-ray diffraction and XAS at the Pt L_3 and L_2 edges indicate that the PtSn/C catalyst has a Pt_3Sn $L1_2$ structure, and alloying with Sn causes partial filling of the Pt d band vacancies and an increase in the Pt–Pt bond distance from 2.77 to 2.8Å. However, upd Sn does not perturb Pt structurally or electronically. XAS at the Sn K edge indicates that both the upd Sn on Pt/C and the surface Sn on PtSn/C are associated with oxygenated species at all potentials and that the nature and strength of the Sn–O bonds are potential dependent. The differences in the activity of the two catalysts for the MOR are due to the effects of alloying on the Pt electronic structure that inhibit the ability of the Pt to adsorb methanol and dissociate C–H bonds." [13]

X-ray standing wave technique

The standing wave technique is a very sensitive method for determining the position of atoms adsorbed onto a single-crystal electrode. It is based on the interference between the incident and the Bragg diffracted beams from a perfect crystal. The standing wave not only exists in the crystal but also extends about 1,000Å above its surface. The spacing of the planes in the crystal determines the distance scale over which the adsorbate can be probed. The nodal and antinodal planes of the standing waves are parallel to the planes in the crystal, and they move as the angle of incident beam is changed. Consequently, for an atomic overlayer, which is parallel to the crystal planes, the nodal and antinodal planes of the standing wave will pass through the atomic plane as the angle of incidence is varied and the fluorescence emission yield from atoms in the overlayer will be modulated in a characteristic fashion.

One disadvantage of the standing wave technique is that it requires a perfect-single-crystal electrode. Furthermore, the periods of the standing wave generated from a single crystal are too short to investigate surface structures extending much further than the crystallographic d spacing, for example, to investigate the ionic distribution in the electrochemical double layer ranging from a few tens to hundreds of angstroms. Thus, an alternative type of substrate must be used to create standing waves with long periods. Such investigations can be carried out using a layered synthetic microstructure (LSM) electrode. These are artificial, depth-periodic structures, consisting of alternating layers of high and low electron density elements, thus creating a superlattice structure with diffraction planes centered in the high electron density layers, for example, a Pt/C LSM with a d spacing of 40.8Å and Pt as the surface material (Fig. 9).

Surface adsorption and corresponding diffuse-double-layer structure determination

An example is the determination, in situ and with angstrom resolution, of the potential-dependent density and distributional changes of iodide at the Pt surface using the LSM shown in Fig. 9, from a solution of 0.1 M Na_2SO_4 containing 10^{-5} M NaI [14]. The data were interpreted using a simple model consisting of an adsorbed adlayer and an exponentially decaying diffuse layer. It was shown that the decay length of the diffuse layer increased smoothly from −0.1 to +0.4 V, followed by an abrupt decrease at the highest potential investigated. In contrast, exactly the opposite behavior was found for the fractional concentration (the ratio of the initial number concentration of iodide in the diffuse layer and the number concentration of adsorbed iodine adatoms). What was most remarkable in these results is the magnitude of the variations in these parameters with potential, especially in light of the fact that iodide is present in a solution containing a large excess of sulfate dianion supporting electrolyte (Fig. 10).

Surface X-ray scattering

Surface-X-ray scattering can be categorized into three types, namely, X-ray reflectivity, glancing angle in-plane

Fig. 9 Illustration of the X-ray standing wave generated using a platinum/carbon LSM. The *dashed lines* mark the position of the diffraction planes in the multilayer (Reproduced with permission from Ref. [14], Copyright 1990 by American Chemical Society)
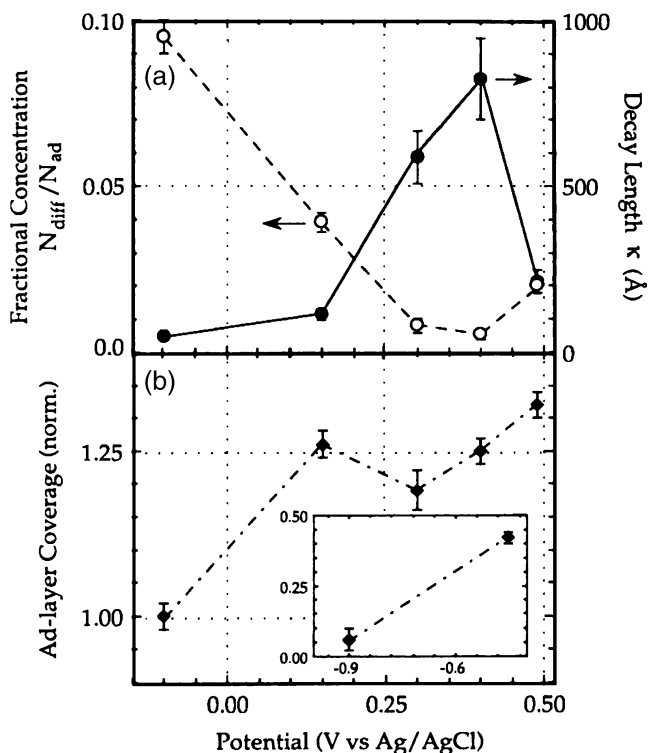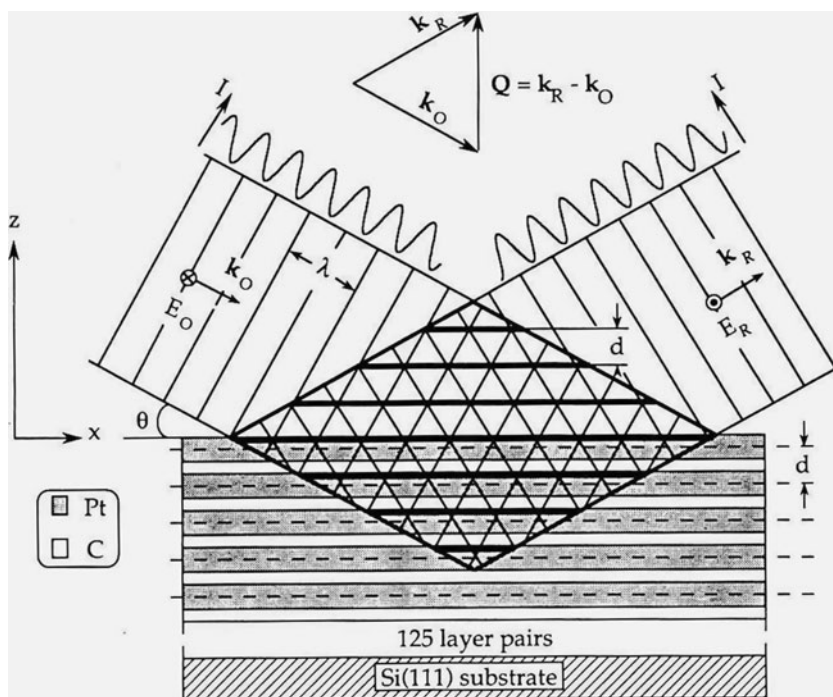

Fig. 10 Plot of **a** the diffuse layer decay length (*filled circles*), the fractional concentration N_{diff}/N_{ad} (*open circles*), and **b** the normalized adlayer coverage as a function of applied electrode potential. The *inset* plots the normalized adlayer coverage at the extreme negative potentials studied (Reproduced with permission from Ref. [14], Copyright 1990 by American Chemical Society)

X-ray diffraction, and crystal truncation rod (CTR) measurements. (1) The specular and off-specular X-ray-reflectivity techniques are used to study surface morphology. They are not typically sensitive to crystalline structures of the surface but sensitive to nano- to micrometer length scales. (2) Glancing angle in-plane diffraction, measured parallel to the surface with incident and diffracted X-rays at glancing angles, is extremely sensitive to the two-dimensional structure and reconstruction. (3) Crystal truncation rods (CTR) (described below), measured normal to the surface, are extremely sensitive to the surface coverage and relaxation.

X-ray diffraction examination of bulk crystal structures is an old, established technique resulting in the well-known diffraction pattern of Bragg points (peaks). These diffraction peaks originate from scattering points that are surrounded in all directions by a repeating structure. The situation is different when the symmetry is broken by a sharp termination of the crystal at its surface, since one half of the structure that would be above the surface is eliminated. The diffraction from the truncated structure is much weaker than that that form the bulk, and it appears between the Bragg points along directions normal to the surface. This scattered signal is typically called a CTR. This has been known, at least in principle, since the time of Bragg, but the practical use was greatly hampered by the weak signal until the availability of synchrotron sources starting in the late 1970s. As the example in Fig. 11 indicates, the reflected intensity is many orders of magnitude lower than at the Bragg peaks.

X-ray scattering has been used for the investigation of a large variety of phenomena in the electrochemical inter-
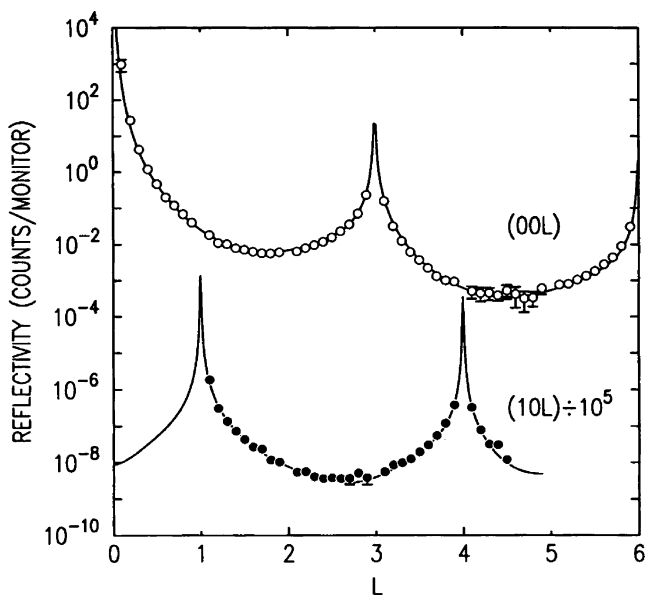
Fig. 11 X-ray intensity along the crystal truncation rods from a clean platinum surface under 0.1 M perchloric acid [15]

phase during the last 25 years. The areas investigated include the roughness of electrode surfaces including relaxation/reconstruction of metal surfaces; the structure of the electrochemical double layer; adsorption/absorption at electrode surfaces; kinetics/mechanism and catalysis of charge-transfer reactions; metal deposition at the submonolayer, monolayer, and multilayer level; compound deposition and deposition by electrochemical atomic layer epitaxy; oxide film formation on metals and passivation, corrosion and metal dissolution; and porous electrode surfaces such as anodic formation of porous silicon. In addition to metal/aqueous solution interfaces, some work was also carried out on liquid metal, semiconductor, and bulk conducting oxide electrode surfaces and at metal/polymer electrolyte and immiscible liquid/liquid interfaces. More than 200 such applications of the scattering technique are listed in a recent, extensive review [9]. A limitation of the technique is that the best results are obtained with high-quality single-crystal electrodes; only a few of the listed applications are on polycrystalline electrodes. A few examples will be briefly described here.

Oxidation/reduction of platinum electrodes

*Surface roughening during the incipient stages of oxide formation*

Experiments in 0.1 M CsF solution have shown that the surface irreversibly roughens when the potential is cycled beyond 1.3 V (HE, potential of hydrogen evolution), while the initially flat surface can be completely recovered after

electrochemical reduction of the oxide film formed at potentials more negative than 1.3 V [16]. A series of normalized crystal-truncation-rod scans is shown in Fig. 12. Each scan was made at 0.8 V, after oxidation at the potential indicated and reduction at 0.0 V. All data are divided by the 0.8-V data to emphasize the surface contribution, and each scan from the top is offset sequentially by an order of magnitude for display purposes. The abscissa is the reciprocal lattice unit of platinum in the hcp unit cell. Electrochemical measurements (cyclic voltammetry) of the oxygen coverage of the platinum surface indicated that a full monolayer of oxide coverage was not achieved at potentials negative to approximately 1.4 V, suggesting that oxidation/reduction of less than a monolayer of oxide film will not destroy the originally flat surface, but the surface will roughen if more than a monolayer of oxide is formed/reduced.

The roughness of the surface atomic layers could be determined by comparing the experimental data to predictions of the scattering equation applied with some simple models of rough surfaces (Fig. 13). In these calculations, only occupational disorder was considered. The experimental data are compared with curves calculated from the various models in Fig. 14. It is quite evident that only the three-step model fits the data.
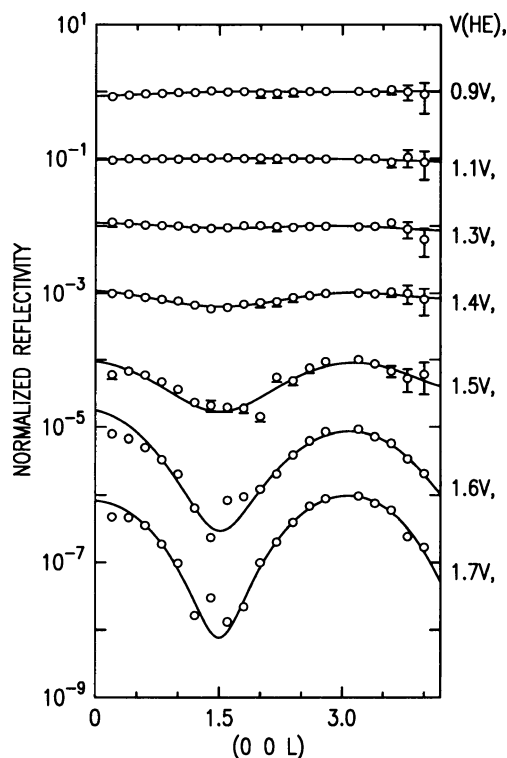

Fig. 12 Crystal-truncation-rod scans of Pt(111) oxidized at potentials indicated. *Open circles* represent the experimental data, and the *solid lines* were calculated with the three-step model (Fig. 13) [3]
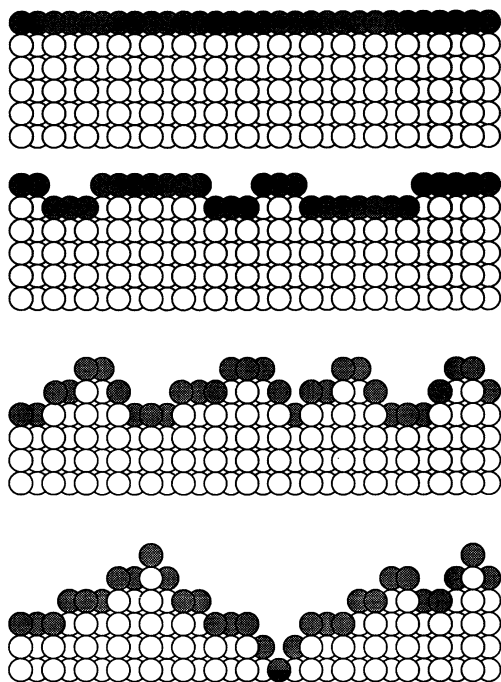
Fig. 13 Surface roughness models. From *top* to *bottom*: ideal surface, two-step model, three-step model, and multiple-step model. The *shaded circles* represent platinum atoms exposed to the solution [17]

Oxide film formation and dermasorption of oxygen

X-ray scattering was also used to investigate many other aspects of the submonolayer/monolayer oxidation/reduction of platinum [9, 17]. It was found (see Figs. 15 and 16) that there are three distinctly different behaviors that can be best separated in terms of the total amount of charge transferred during the surface oxidation (expressed in units of "number of electrons transferred per surface platinum atom," e^-/Pt). (1) Up to approximately 0.6 e^-/Pt (~0.9 V, HE), there was no change in the X-ray scattering in spite of the obvious
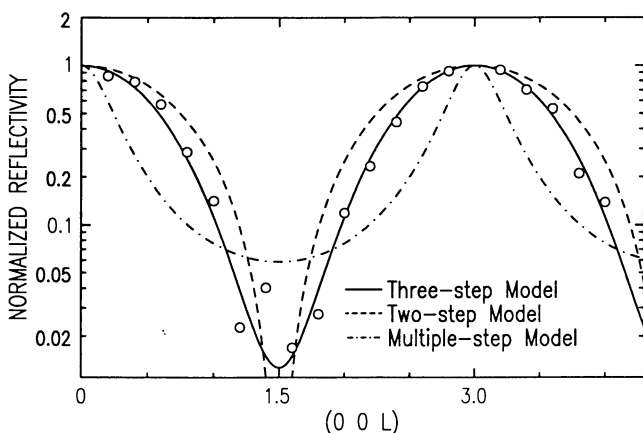

Fig. 14 Normalized reflectivity data and comparison with models for a reduced surface obtained after oxidation to 1.7 V in CsF solution [16]
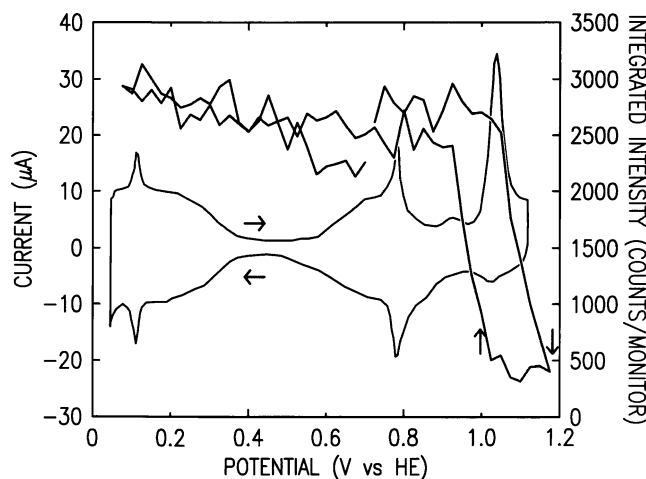
Fig. 15 Voltammogram of Pt(111) in 0.1 M $HClO_4$ solution (*bottom curve*) and the change of scattered X-ray intensity at (0, 0, 1.3) versus potential (*top curve*). The potential scale is referenced to the potential of the beginning of hydrogen evolution in the CV [17]

electrochemical indication of surface oxidation. (2) Between approximately 0.6 and 1.7 e^-/Pt (up to approximately 1.2 V), an increasing deviation was found from the scattering measured at oxide-free surfaces. However, upon electrochemical reduction of the surface, the original oxide-free surface scattering was always reproduced, indicating that the surface processes were completely reversible. (3) Oxidation for >1.7 e^-/Pt irreversibly changed the X-ray scattering, indicating an irreversible roughening of the surface.
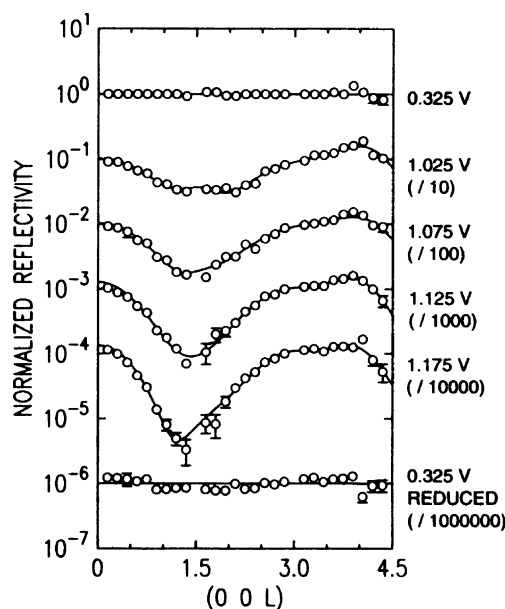
Fig. 16 (00 L) scans of Pt(111) in 0.1 M $HClO_4$ solution, normalized to the oxide-free scan. The scans are offset for clarity. The potential was changed to four consecutively more oxidizing potentials between 1.025 and 1.175 V (HE). Finally, the surface was reduced, and the final X-ray measurements indicated that the original smooth surface was recovered. The *lines* are fits with the place-exchange model [16]

The following explanation of these observations was proposed. (There is a caveat that only the positions of the Pt atoms can be considered in the modeling of the X-ray scattering because the electron densities of both the OH$^-$ and O^{2-} species are negligible compared with that of Pt. Therefore, X-rays cannot distinguish between the OH$^-$ and O^{2-}, nor can they be used to determine directly the position of these species.) During the first phase of surface oxidation, either the OH$^-$ or O^{2-} was chemically adsorbed onto the surface without changing the structure of the underlying platinum. These structures represent dipoles and, because of the high repulsive dipole–dipole interaction energy, adsorption occurred in "nearest-neighbor-avoiding" configuration till at a critical point of coverage, some of the dipole structures were flipping around resulting in "place exchange" (sometimes called *dermasorbed oxygen*). Modeling of the X-ray-scattering data indeed gave the best fit with the place-exchange model (Figs. 16 and 17). The fraction of place exchanged platinum atoms increased linearly from about 0.21 to 0.33 for the four scans shown in Fig. 16. At this phase of the oxidation, it was possible to essentially recover the original smooth platinum surface with cathodic reduction of the oxide layer. The proposed consecutive surface structures are shown in Fig. 18.

Once a full monolayer of the place exchanged structure was completed (at the oxidation of 1/3 of the platinum atoms in the surface), upon further oxidation, OH$^-$ or O^{2-} reacted with the *place-exchanged* Pt atoms. Therefore, the formation of the Pt–O or Pt–OH (shown in the boxes in Fig. 18) was accompanied by a decrease of the metal–oxygen bond strength in the second layer of platinum atoms. Consequently, the newly formed Pt–O or Pt–OH
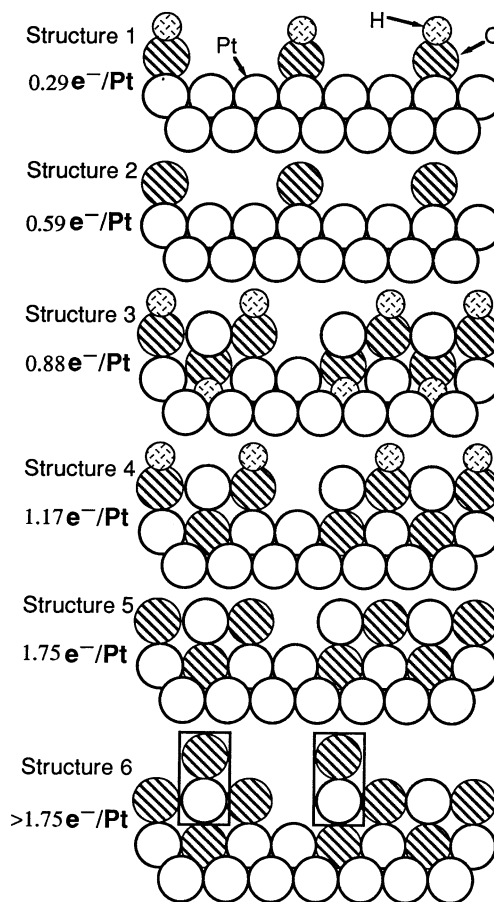

Fig. 18 Six possible structures of the oxidized surface [17]

would easily move away from their original positions by surface diffusion, and reduction of the oxide would not recover the original Pt surface structure, resulting in irreversible roughening of the surface.
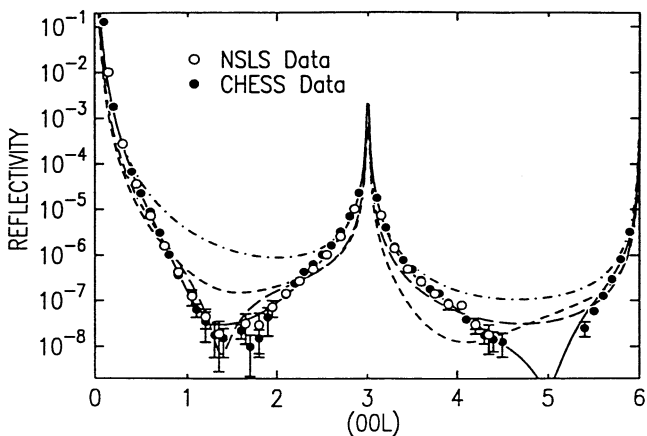
Fig. 17 The (00 L) scan at 1.175 V with fits based on several models. (The data reproducibility is indicated by the good agreement between datasets taken at two different synchrotrons.) *Dot-dashed*, ideal surface; *long-dashed*, buckled surface; *short-dashed*, ClO$_4^-$ adsorption; *solid*, place exchange [16]

Fig. 19 Best fit of the CTR data for the normalized oxygen distribution of water near a Ag(111) electrode surface as a function of the distance above the top silver atomic plane (Reproduced with permission from Ref. [18], Copyright 1995 by Elsevier)

Double-layer structure studies

Water at the silver surface

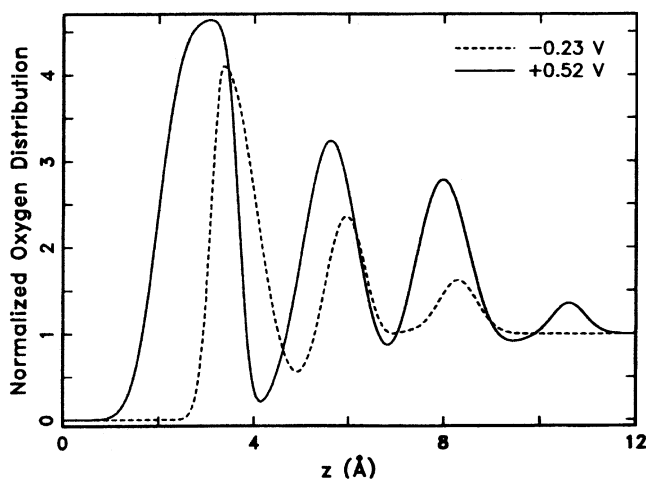The investigation of the water structure at the Ag(111) produced some unexpected results [18]. No "ice-like" structures were found, and the main features concluded from the oxygen distribution (Fig. 19) were the potential dependent layering of the water molecules extending to about three molecular diameters with a reorientation of the water as a function of potential. What was unexpected was the density of the water molecules in the first layer: 1.1 (at −0.23 V to pzc) to 1.8 (at +0.52 V) per silver atoms. One would expect ~0.8 water molecules per silver atom. This high surface density of water was tentatively explained by the effect of the large electric field (~10^7 V/cm) at the surface of the electrode.

Water at the ruthenium dioxide surface

A different picture emerged from a study of ruthenium dioxide(110) single crystal electrodes [19]. There are special characteristics of this facet that make its study especially informative: Certain crystal truncation rods are dominated by scattering from oxygen atoms only (called further as "oxygen-rods") due to the fortuitous cancellation of the signal from the two Ru sublattices, while most other rods are typically dominated by the much heavier ruthenium atoms. Cyclic voltammogram and X-ray-intensity data (Fig. 20) indicated a complex behavior, including oxidation/reduction of the electrode and the beginning of oxygen evolution.
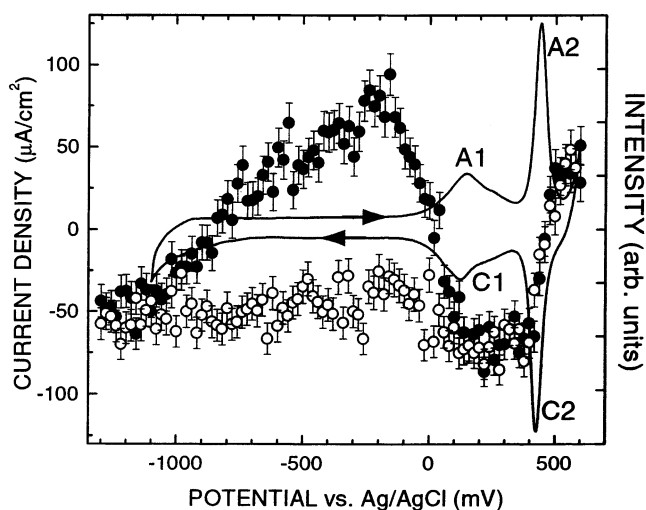
Fig. 20 Cyclic voltammogram (*solid line*) and X-ray intensity (*circles with error bars*) at (014) measured for the RuO_2(110) surface in 0.1 M NaOH. *Filled* and *open circles* are for cathodic and anodic sweeps, respectively. The *arrows* indicate the directions of the potential change [19]

However, the most interesting feature of these changes was the formation of a commensurate water layer on the surface with a structure very closely resembling that of "ice X." The X-ray intensity near the Bragg peaks was very strong in the truncation rods because the X-ray-scattering amplitudes from many layers are added in-phase, but this signal was insensitive to the surface structure. The intensity distribution around the anti-Bragg point (mid-point between two adjacent Bragg peaks) was typically weak and concave because X-rays scattered from different layers were out of phase, but it was sensitive to the positions of surface atoms. For instance, if a new layer would form over an ideal termination at a height twice the bulk spacing, the scattered X-ray amplitude from the new layer would be added in-phase and the anti-Bragg point would change from a minimum to a local maximum. Therefore, the concave-to-convex change in the off-specular oxygen rods, seen in these measurement near the anti-Bragg point (e.g., (014) and (105) in Fig. 21), demonstrated the possibility of the formation of such an extraneous layer of oxy-species. Additionally, this proved the commensurate nature of the extraneous layer since an incommensurate or disordered layer would not affect the off-specular rods.

The assumed structure of this layer is shown in Fig. 22b. The X-ray scan superimposed on the cyclic voltammetry (CV) in Fig. 20 was one that was very sensitive to this layer. These data agreed with the model of the ice-layer formation as the surface is oxidized; however, there was an interesting hysteresis in the X-ray scattering not present in the CV. Apparently, as the surface was reduced. there existed a "memory effect," and the ice-like water layer structure was retained, although it was not strongly bound to the surface any more. As the potential was swept further negative, this layer was slowly lifted to further and further distance from the surface (Fig. 22c) till it finally disintegrated. On the other hand, on reversal of the sweep in the anodic direction, the ice-like layer could not reform till the surface was oxidized. This is the first instance of the demonstration of an ice-like water structure in the electrochemical double layer.

Ionic distributions at a liquid/liquid interface

A brief experimental note: At a normal synchrotron workstation, the incident angle of the X-ray beam cannot be varied; consequently, the electrochemical cell must be rotated along all three spatial axes, sometimes to a considerably large angle. This cannot be done with a liquid/liquid interface. Fortunately, there are a few special workstations where the incident X-ray beam can be varied within a restricted range.

Fig. 21 RuO$_2$(110) CTRs at (10 L) and (01 L) (oxygen rods) and (20 L), measured at potentials of **a** 330, **b** 500, and **c** −200 mV. *Solid lines* are the results of the best curve fits [19]
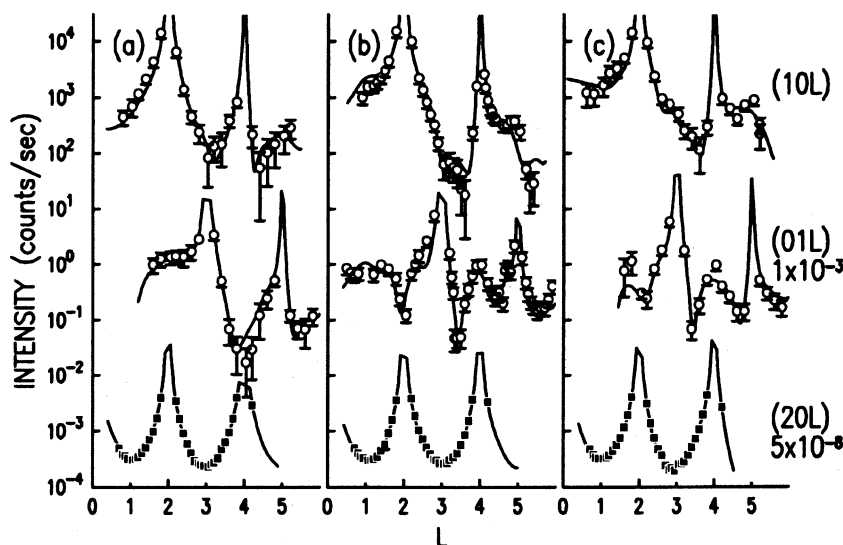

In one investigation of the liquid/liquid interface, the ionic distribution in the diffuse double layer was measured, using the X-ray reflectivity technique, at the nitrobenzene/water interface containing dissolved tetra-butylammonium tetraphenylborate (TBATPB) and tetra-butylammonium bromide (TBABr), respectively [20]. It was concluded that the predictions of the Gouy–Chapman theory, which ignores the molecular-scale structure of the liquid, did not agree with the measurements. In another model, molecular dynamics simulations were carried out, which included the liquid structure, to calculate the potential of mean force on a single ion. Using this potential of mean force in a generalized Poisson–Boltzmann equation to predict the full ion distributions gave an agreement with the experimental results without any adjust-able parameters (Figs. 23 and 24).

Adsorption at electrode surfaces

Adsorption of carbon monoxide on platinum surfaces

The adsorption of CO on the platinum electrode surface is of interest because of its direct relevance to the mechanism of poisoning in modern low-temperature fuel cells. Synchrotron-X-ray-scattering investigations confirmed the existence of a (2×2)–3CO and a (√19×√19)R23.4°–13CO lattice on Pt(111) [21]. The cyclic voltammograms with and without pread-sorbed CO are shown in Fig. 25 in 0.1 M HClO$_4$+10 mM NaBr, together with integrated scattering intensities as a function of potential in a CO-saturated solution. The current peak at around 780 mV (RHE) in the anodic scan (solid line) is due to the oxidation of cc 9% of the preadsorbed CO, which accompanies transition from (2×2) to (√19×√19). This

Fig. 22 Ball-and-stick models for **a** 330-, **b** 500-, and **c** −200-mV structures. The *blue balls* represent the Ru atoms. The *red, orange,* and *yellow* balls represent oxygen atoms in the bulk, on the surface bonded to Ru, and in the water molecules, respectively. The *small green balls* represent the hydrogen atoms, conjectured to show conceivable hydrogen bonds [19]
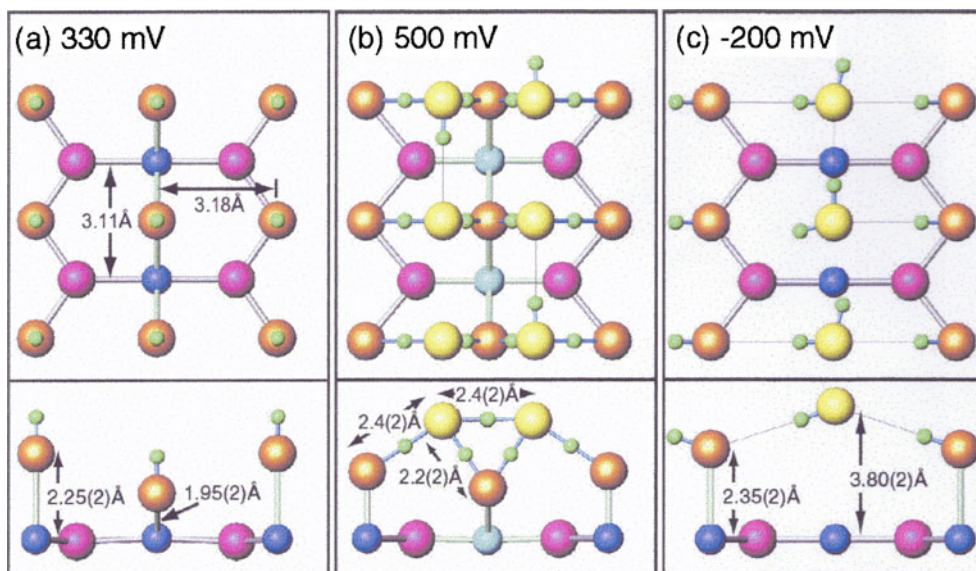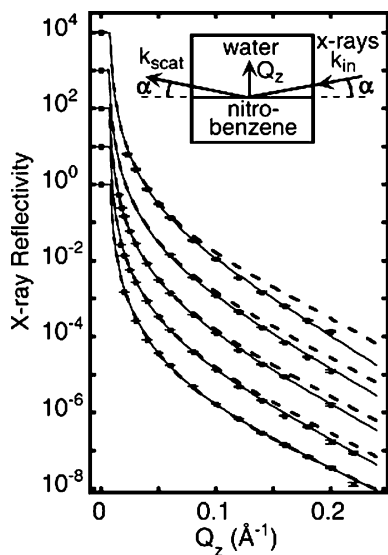
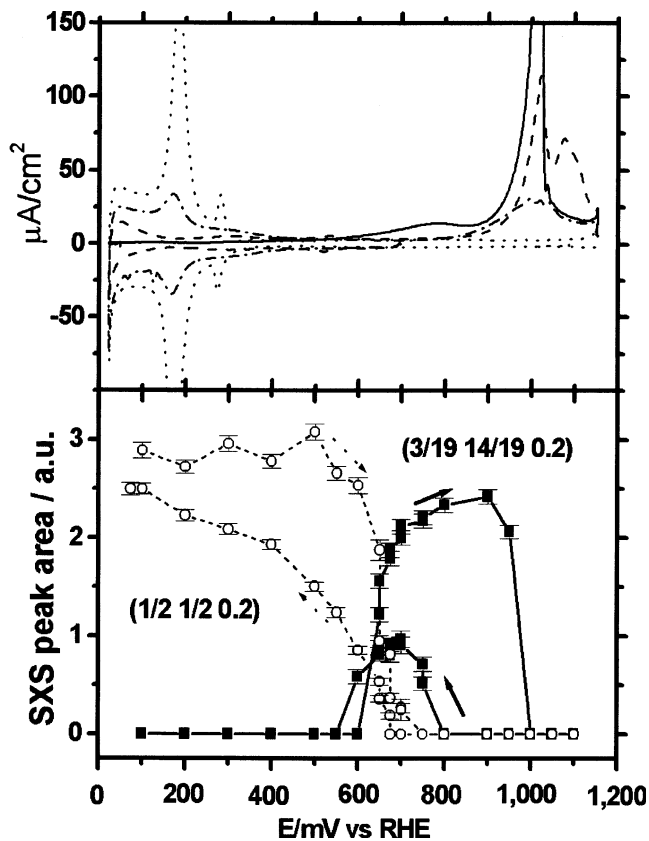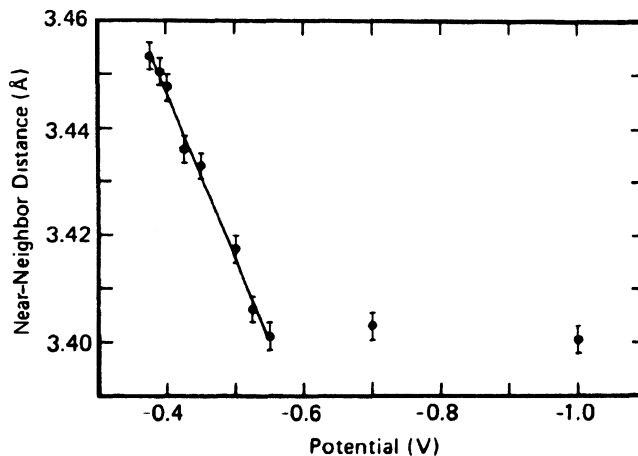**Fig. 23** X-ray reflectivity as a function of wave vector transfer from the interface between a 0.01-M solution of TBATPB in nitrobenzene and a solution of TBABr in water at five concentrations. *Solid lines* are predictions using the potential of mean force from molecular dynamics (MD) simulations. *Dashed lines* are predicted by the Gouy–Chapman model (Reproduced with permission from Ref. [20], Copyright 2006 by AAAS)

Fig. 25 *Top*, CVs (first anodic scans) at 50 mV/s with CO preadsorbed at 50 mV (*solid line*), at 700 mV after 30 min of Ar purge (*dashed*), at 700 mV after 60 min of Ar purge (*dash-dot*), and without preadsorbed CO (*dotted line*). *Bottom*, integrated SXS intensities (*filled triangles*) at (1/2 1/2 0.2) and (*open triangles*) at (3/19 14/19 0.2) as a function of potential in CO-saturated solution. The *vertical size of the symbols* corresponds to *error bars* (standard deviation) of the signal. *Lines* are drawn for visualization only (Reproduced with permission from Ref. [21], Copyright 2004 by The Electrochemical Society)

Fig. 24 Ion distributions at the interface between a 0.08-M TBABr solution in water and a 0.01-M TBATPB solution in nitrobenzene. *Solid lines*, TBA$^+$; *short-long dashed line*, Br$^-$; *short dashed line*, TPB$^-$. **a** Gouy–Chapman theory. **b** Calculation from MD simulation of the potential of mean force (Reproduced with permission from Ref. [20], Copyright 2006 by AAAS)

Fig. 26 Lead–lead near-neighbor distance versus electrode potential (Reproduced with permission from Ref. [22], Copyright 1988 by the American Physical Society)

transition occurs at a less positive potential (650 mV) in the X-ray measurements. This is due to the difference in CO pressure and in the timescale of the two experiments. Whereas the CV was acquired at 50 mV/s, the X-ray data were acquired stepwise with about 4 minutes' time delay. Upon further increase in potential, adsorbed CO is completely oxidized as manifested by the anodic CV peak at 1,020 mV and disappearance of the ($\sqrt{19} \times \sqrt{19}$) reflection at 930 mV. The discrepancy between the values of the CO stripping potential can be again attributed to the different experimental conditions. Upon reversal of the potential scan direction, restoration of the ($\sqrt{19} \times \sqrt{19}$) structure is delayed to 720 mV, showing about 200 mV hysteresis between CO stripping and reordering. Because the CV in the presence of solution-phase CO shows a similar hysteresis between CO oxidation and adsorption peaks, it was concluded that CO does not adsorb on Pt(111) in the potential range between CO stripping and ($\sqrt{19} \times \sqrt{19}$) formation. This hysteresis appears to be an intrinsic phenomenon related to competition between CO and anions for Pt sites, and it is not related to the slow ordering of the ($\sqrt{19} \times \sqrt{19}$) phase.

Underpotential deposition of submonolayer metals

An example is the deposition of lead on Ag(111) [22]. The lead was found to have a close-packed-hexagonal structure, incommensurate with the underlying silver, and rotated 4.5° about the six-fold axis of the silver substrate. An interesting feature of this layer was that it exhibited a two-dimensional compressibility as a function of potential (Fig. 26). The lead–lead interatomic distance decreased linearly with potential until the start of bulk deposition; at more negative potentials, the structure of the UPD layer remained unchanged with a 2.8% contraction from bulk lead. The rotational epitaxy degree did not change with potential. The compression of the structure with potential was tentatively explained by a thermodynamic driving force due to an "ionic overpressure" from the solution.

Structure of anodically formed porous silicon

Roughness of surfaces can also be investigated at a much larger scale than atomic layer level, for example, the investigation of the anodic formation of "porous silicon" layers [23].

The experiments were performed with p^+-type silicon with a resistance of 0.015 Ω/cm, and the (100) surface investigated had an initial roughness of 2 to 3 Å. The electrolyte solution was ~25% HF solution (50% aqueous HF diluted with an equal volume of ethanol). The two main characteristics of specular reflectivity utilized in this work were: (1) the critical angle for total external reflection and (2) the Q dependence of the reflectivity. Diffuse scattering was also used around the Bragg reflections to study the in-plane structure of the pores. One series of reflectivity scans obtained are shown in Fig. 27. The top two scans were carried out before any anodic dissolution. The subsequent scans were made after the application of a successively increasing number of dissolution pulses at 10 mA/cm² resulting in the dissolution of the equivalent of solid silicon layers ranging from approximately 135 to 2,500 Å, for a grand total of 24,000 Å. All the scans were linear for angles larger than the critical angle, and the slope of the reflectivity scans changed during the first few successive dissolutions but remained constant thereafter. In other words, the interface density profile reached a steady-state functional form at a critical dissolution depth (~300 Å of solid silicon for this particular set of data). This observation indicated the existence of an interfacial region where the density gradually changed, followed by another layer where dissolution in excess of a critical depth did not significantly alter the density profile any more. Furthermore, this observation also indicated that the interface density profile should follow a power law. The critical angle was well defined for all the scans, and it decreased continuously as the total dissolution amount increased. The critical angle of the top two scans (zero porosity) was 0.025 Å⁻¹, and it decreased to 0.018 Å⁻¹ for the last scan (indicated by the arrows in Fig. 27). The porosity of silicon could be estimated from the measured critical angles. For example, the porosity of the last scan was approximately 52%. This porosity was averaged over a depth of 1.4 μm, which was the penetration depth of X-rays at the critical angle.

Two possible pore distribution models consistent with the power-law density profile (1) tapered pores with relatively uniform length across the sample surface and (2) pores with
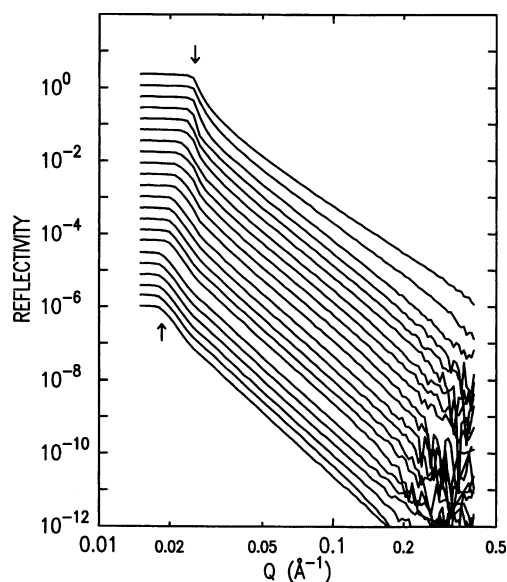
Fig. 27 A series of reflectivity scans during anodic oxidation of silicon. The scans are offset from each other for display purposes [23]

uniform radius and a length distribution matching the overall power-law interfacial-density profile. The reflectivity data were consistent with either possibility or with any combination of them. Therefore, additional measurements were made for diffuse scattering around the Bragg reflections to determine which model was closer to the real structure of the pores. It was found that a funnel-shaped (tapered) interfacial layer, followed by a layer of uniform porosity with relatively straight circular pores and increased branching with depth, provided the best fit to the data. For the particular conditions, the porosity was around 50%, and the pore diameter was about 50 to 70Å. It was also found that the space–charge regions became "insulating" layers between the pores, because the holes must overcome the potential barrier of the space–charge region for the dissolution process to continue. To illustrate this, schematic views of pore cross sections at a given depth are shown in Fig. 28a; it illustrates the mechanism of pore "repulsion." The arrows represent growth rates, the white area is space–charge region, and the gray background is solid silicon. Holes cross freely in the direction of the long arrows, but fewer hole crossings are possible across the space–charge region in direction of the short arrows. Consequently, a pair of holes will grow apart, thereby, avoiding the overlap between nearest neighbors. Figure 28b illustrates the termination of lateral growth of the pores. The growth of the pores towards each other will be terminated when three pores meet. Only three pores are shown for illustration purposes, but lateral growth of pores will be similarly terminated when all pores are closely packed.

Applications of the far-infrared range of synchrotron radiation

As mentioned earlier, the synchrotron generates electromagnetic waves in a continuous and wide range of frequencies, including the infrared region. Infrared spectroelectrochemistry has been widely used to investigate the electrochemical interphase, most importantly to provide information on the identity and orientation of adsorbed molecules. Experiments

carried out with traditional, thermal sources are often brightness limited, especially in the far-infrared region (<750 cm^{-1}), which can provide direct information on the metal-adsorbate bond and on the electric field strength within the first 1–2Å of the metal surface. The far-infrared radiation at synchrotrons is about thousand times as bright as the traditional sources, making such experiments practical. For example, the influence of the adsorption of fluoride on the bonding of water to a silver electrode surface has been studied by observing the Ag–O stretching vibration in the far-IR [24].

Some historical notes and personal reminiscences

The so-called first-generation synchrotrons were designed, built, and operated for high-energy physicists. It was sort of an afterthought that these "machines" (as they are usually called) could also be used as X-ray sources since they did generate X-rays as a completely unintended side effect of their operation. These powerful X-rays promised to be a bonanza for chemists, biologists, crystallographers, etc., as compared with X-ray power available in their laboratory sources. However, these applications were considered "parasitic uses" and, indeed, were treated as such as far as available facilities, beam times, and convenience of use were considered. But, they proved the very high experimental value of these X-ray sources. Subsequently, machines were designed, built, and operated with their only purpose to be dedicated X-ray sources for any scientific discipline. The cost of such a machine is of the order of hundreds of millions of dollars. These second-, third-, and now fourth-generation synchrotrons were built to be powerful, practical, and "user-friendly" X-ray sources for the wide variety of X-ray techniques to be used across a wide variety of scientific disciplines, among them, electrochemistry.

There have been tremendous improvements during the last decades. Let me just emphasize one aspect. At one first-generation machine, the standard operating routine was 50 min of beam, followed by 10 min of some adjustments, repetitively. Unfortunately, during the first 10 to 20 min

Fig. 28 Schematic diagrams for pore formation: *a* pore "repulsion" and *b* termination of lateral growth [23]
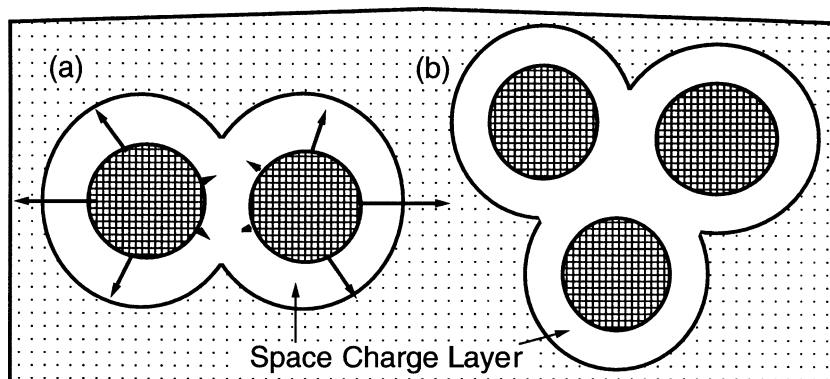
after startup, the beam was unstable, and, consequently, we had about 30 min of measuring time during every hour. This required some precarious planning for our experiments. The second-generation machines were much better. The operating times were measured in hours (hoping for 12 h, but seldom achieving this in the early years), followed by a couple of hours of "refill." Unfortunately, the beam intensity declined continuously during operation, making it necessary to somehow normalize every single measuring point. By now, they fairly routinely run for around 24 h. The third-generation machine was a quantum leap improvement. The beam intensity was kept practically constant by frequent "top-offs," which were transparent to most users, and the beam could be available for days and days, continuously. Of course, all this refers to ideal conditions. The synchrotrons are very complex machines, as are the beam lines and the X-ray equipment. All are subject to periodic breakdowns (not to mention the breakdown of your electrochemistry setup). In the beginnings, often you were lucky if you could use half the time you thought you had. Luckily, reliability is much improved lately.

My first introduction to synchrotron life came during a "user meeting" that I attended before we started to make trips to the synchrotron. As part of that meeting, they took us on a tour of the experimental area. I was duly impressed by all the blinking lights, CRT displays, knobs, switches, and dangling cables crammed into small places, looking like the inside of a space capsule. But the most telling aspect, as I indeed found out later, came when we walked by a small snack room, strategically located in the middle of the experimental area. In addition to coffee, coke, and snack machines, it contained a fairly large, round table with a number of chairs around it. On the table lay a fellow, spread out on his back, snoring away merrily. This was in the middle of the afternoon, surrounded by busy experimental stations with large number of people milling all around. Well, I never utilized this "facility" later, though I tested it briefly but found its surface to be too hard for my liking.

So how does one start to work at a synchrotron? First, you write a proposal on what you want to do and why. If everything goes well, you then get assigned some "beam time" at some "beam line" in the future. Depending on the type and complexity of your measurements, this may be 2–3 days, or a week or two. This short, fixed time frame is one of the defining aspects of synchrotron work. At home, if your experiment does not work out today, maybe it will work tomorrow or next week. At the synchrotron, if your experiment does not work out within your allotted time, you are out of luck till your next trip, which may be 6 months away. So, you better be well prepared and use the time effectively. The synchrotron, at least in principle, operates 7 days a week, 24 h a day, and you try to use every single minute of your time to squeeze out as many data points as you can. So, you try to arrange for a team of people to be able to work in shifts. This does not always work. First of all, not necessarily everyone in the team can handle every task, so in cases of emergencies (which seem to be the normal situation) you may have to wake up your friend in the nearby motel to get help. Also, once you really start to get interesting data, people usually become excited and everybody wants to be there to see what is happening. Well, you may get by for 2–3 days with a few hours of sleep, but it gets hard for a 2-week beam time. This is when the snack-room tables come in handy. And the library! Every synchrotron I have used has a local library as part of the experimental floor. I spent many-many hours in these libraries, but I can recall only one, maybe two, instances when I saw somebody using a journal or book from the collection. These libraries are strategically equipped with several soft reclining chairs and sofas, and at any hour of the day or night you will find people making good use of them. The extreme case I saw during one of our trips was at a neighboring beam line where a graduate student was working, apparently without any help. Amongst his several instrument racks he had a nice long table with a camping type cot underneath. With the help of this and a large and loud alarm clock, he was living at the beam line during his experimental time. Yes, I know that at most laboratories (especially at universities) the day is not 8 h, but it is seldom 20 or 24 h.

The second defining aspect of synchrotron work is that the synchrotron is probably hundreds, maybe even thousands, of miles away from your home base. So, you plan your experiments carefully and plan what equipment you need to take with you. Here, electrochemists are at a disadvantage; some solid-state physicists put a single crystal in their pocket and are ready to fly. We need gas sources, solution sources, and at ultra-high purity. Chemicals, solids, liquids, and gases must be purchased or shipped, and gas-purification and solution-purification equipment, potentiostats, etc. all have to be shipped back and forth. And, these are only the major equipment. All synchrotrons have of course stock rooms, filled with bolts and nuts and electronic equipment, but just try to find a medicine dropper or pH paper! With some luck, a chemistry stock room will be somewhere not too distant, but these are open Monday to Friday from 9 am to 5 pm. If your hydrogen-gas cylinder runs empty in the middle of a 4-day weekend, you do strange things that better remain unrecorded. This may seem a trivial problem, but it is not. It is amazing how many little things you need during an experiment that are readily available for you at home in your drawers and cupboards, so you never give them a thought until you do not have them, from hose clamps to pipettes and beakers, the most mundane things! However, it only takes practice, after a few trips you develop your "must-have" list. But, it can be a long list! For some of our trips, we rented a large commercial

van and filled it completely. Also, necessity is the mother of inventions, and it is interesting how you can find that laboratory equipment can be used for dozens of purposes for which they were never intended. And finally, but not least, having good friends who are residents at the institution where the synchrotron is located is an absolute blessing.

Electrochemists have one more difficulty at synchrotrons. At a normal workstation, the incident angle of the X-ray beam cannot be varied; consequently, the electrochemical cell must be rotated along all three spatial axes, sometimes to a considerably large angle. This requires special cell designs to maintain electrolyte coverage of the electrodes and avoid spilling the electrolyte at practically any angle of rotation. Cell design details are described in a recent review [9]. Furthermore, once the X-rays are on, no one can enter the experimental enclosure (the "hutch"); consequently, all electrochemical manipulations and data collections must be carried out under full computer control, with the same computer that controls the X-ray equipment.

With all these trials and tribulations, I have found our synchrotron trips very interesting, exciting, and scientifically productive. You have together a group of people with one and only one single-minded purpose: to get the experiments done successfully. The usual distractions are absent, no phone calls, seminars or meetings, no report deadlines. You spend practically all day together (say, 20 h of it), have breakfast together, have lunch and dinner together, and talk about all things (from politics to sports) but mainly science. What did the last experiment mean? What do we do next? Occasionally wild ideas come along. It is a tiring, but very concentrated, intense, and exciting group effort, something I have never experienced in "normal" laboratory work. Interestingly, and unexpectedly, once our "local" synchrotron was built and we did not need to travel any more, I found this intensity to decline; being at home, there are more distractions and less togetherness. So, there is a trade-off between the complications of travel and the intense group effort.

Concluding remarks and future trends

It was the intent of this paper to demonstrate the usefulness of synchrotron techniques for the in situ investigation of a wide range of phenomena occurring in the electrochemical interphase, in the interphase that extends from a few angstrom to a few thousand angstrom in both the electronically and the ionically conducting phases. The phenomena that can be investigated include, among others, the morphological and chemical nature of the solid interface, adsorption and absorption occurring at the interface, the structure of the electrochemical double layer, and the deposition/dissolution and oxidation of metal interfaces. Many interphases other than

those occurring between a solid metal and an aqueous solution can also be investigated. These in situ measurements were made possible by the advent of synchrotrons, which provide X-rays and infrared radiation orders of magnitude more brilliant than prior sources. While experiments at synchrotron beamlines can be difficult, time consuming, and sometimes frustrating, the results, which usually cannot be obtained with any other technique, are making them worthwhile.

Present synchrotrons are continuously upgraded, and new ones are planned with further increase in the brilliance of X-rays by about two orders of magnitude. This will make the sensitivity achievable even better, make the experiments faster, and make it easier to do kinetic studies. (The storage ring holds the electrons/positrons in orbit in bunches allowing time studies.) In addition to the continuous improvement of synchrotrons, the investigation techniques are also evolving. For example, the recent development of the resonance elastic and inelastic X-ray scattering processes for fluorescence emission and resonance-fluorescence processes makes possible to gain local and *chemical* information of buried electrochemical interfaces not obtainable by any other means [25]. When fully developed, the chemical sensitivity and selectivity of these techniques will permit the study of even weekly adsorbed and light elements at the electrochemical interphase.

References

1. Froment M (ed) (1983) Passivity of metals and semiconductors. Elsevier, New York
2. Abruna HD (ed) (1991) Electrochemical interfaces: modern techniques for in-situ interface characterization. VCH, New York
3. You H, Nagy Z (eds) (1993) Application of X-ray scattering techniques for the study of electrochemical interphases. In: Current topics in electrochemistry 2. Research Trends. Trivandrum, India, pp 21–43
4. McBreen J (1995) In situ synchrotron techniques in electrochemistry. In: Rubinstein I (ed) Physical electrochemistry: principles, methods, and applications. Marcel Dekker, New York, pp 339–391
5. Wieckowski A (ed) (1999) Interfacial electrochemistry: theory, experiment and applications. Marcel Dekker, New York
6. McBreen J (ed) (2002) X-rays in electrochemistry. Electrochim Acta 47:3035–3207
7. Nagy Z (2004) Electrochemistry at synchrotrons. In: Leddy J, Birss V, Vanysek P (eds) Historical perspectives on the evolution of electrochemical tools. Electrochemical Society, Pennington, pp 235–240
8. Sun SG, Christensen PA, Wieckowski A (eds) (2007) In-situ spectroscopic studies of adsorption at the electrode and electrocatalysis. Elsevier, Amsterdam
9. Nagy Z, You H (2009) Application of synchrotron X-ray scattering techniques for the investigation of electrochemical interphases. In: White RE (ed) Modern aspects of electrochemistry no. 45. Springer, New York, pp 247–335
10. McBreen J (1995) In: Munshi MZA (ed) Handbook of solid state batteries and capacitors. World Scientific, Singapore, pp 57–78
11. Virtanen S, Schmuki P, Isaacs HS (2002) Electrochim Acta 47:3117–3125
12. Russell AE, Rose A (2004) Chem Rev 104:4613–4635

13. Mukerjee S, McBreen J (1999) J Electrochem Soc 146:600–606
14. Bommarito GM, White JH, Abruna HD (1990) J Phys Chem 94:8280–8288
15. Nagy Z, You H, Yonco RM (1994) Rev Sci Instrum 65:2199–2205
16. You H, Zurawski DJ, Nagy Z, Yonco RM (1994) J Chem Phys 100:4699–4702
17. Nagy Z, You H (2002) Electrochim Acta 47:3037–3055
18. Toney MF, Howard JN, Richer J, Borges GL, Gordon JG, Melroy OR, Wiesler DG, Yee D, Sorensen LB (1995) Surf Sci 335:326–332
19. Chu YS, Lister TE, Cullen WG, You H, Nagy Z (2001) Phys Rev Lett 86:3364–3367
20. Luo G, Malkova S, Yoon J, Schultz DG, Lin B, Meron M, Benjamin I, Vanysek P, Schlossman L (2006) Science 311:216–218
21. Tolmachev YV, Menzel A, Tkachuk AV, Chu YS, You H (2004) Electrochem Solid State Lett 7:E23–E26
22. Melroy OR, Toney MF, Borges GL, Samant MG, Kortright JB, Ross PN, Blum L (1988) Phys Rev B38:10962–10965
23. You H, Nagy Z, Huang K (1997) Phys Rev Lett 78:1367–1370
24. Russell AE, Lin AS, O'Grady WE (1993) J Chem Soc Faraday Trans 89:195–198
25. Chang KC, Menzel A, Komanicky V, You H, Inukai J, Wieckowski A, Timofeeva EV, Tolmachev YV (2007) In: Sun SG, Christensen PA, Wieckowski A (eds) In-situ spectroscopic studies of adsorption at the electrode and electro-catalysis. Elsevier, Amsterdam, pp 383–407